Reaction 7 demonstrates the stereospecific nature of these reductions using $DW(CO)_5^-$; only the exo isomer (δ 1.49) is formed. Reaction 8 demonstrates the selectivity of these reductions; as noted elsewhere,[7] primary halides are reduced more readily than are secondary halides.

Summary

The anionic group 6B carbonyl hydrides undergo a facile exchange of deuterium for hydrogen with the reagents CH_3OD, D_2O, and CH_3CO_2D. This affords a convenient synthesis or in situ source of the deuterides. Labeling the hydrides with deuterium in this way does not cause changes in the CO region of the infrared spectra of the hydrides, suggesting that the CO and M–H/D stretching vibrations are not coupled in these complexes.

The ability to undergo H/D exchange has been shown to be general for a large variety of terminal hydrides. In contrast, the bridging hydride ligand does not generally exchange with CH_3OD or D_2O, with the exceptions noted in the Discussion. When a large excess of exchange reagent is used, hydrogen elimination (leading to dimer formation) becomes observable, although in all cases H/D exchange occurs more readily. The decomposition by acids of the monomeric hydrides via hydrogen elimination is faster in the order: $HBF_4 > CH_3CO_2H > PhOH > H_2O > CH_3OH$. A common anion-stabilized dihydride intermediate or transition state is proposed both for H/D exchange and for the slower H_2 elimination processes.

The facile exchange of the hydrides with CH_3OD or with D_2O affords a convenient in situ source of the deuterides $DM(CO)_4L^-$ for either spectroscopic studies or for deuterium transfer (sometimes selectively and/or stereospecifically) to organic halides.

Acknowledgment. The financial support of this work by the National Science Foundation (to M.Y.D. CHE-8304162) and the Robert A. Welch Foundation is gratefully acknowledged.

Registry No. $HCr(CO)_5^-$, 18716-81-9; *cis*-$HCr(CO)_4P(OMe)_3^-$, 89210-44-6; $HW(CO)_5^-$, 77227-36-2; *cis*-$HW(CO)_4P(OMe)_3^-$, 82963-27-7; $DCr(CO)_5^-$, 90900-59-7; *cis*-$DCr(CO)_4P(OMe)_3^-$, 90900-60-0; $DW(CO)_5^-$, 89210-45-7; *cis*-$DW(CO)_4P(OMe)_3^-$, 90900-61-1; $HFe(CO)_4^-$, 18716-80-8; CH_3OH, 67-56-1; CH_3CO_2H, 64-19-7; H_2, 1333-74-0.

Molecular Environment Effects in Redox Chemistry. Electrochemistry of Ether-Linked Basket-Handle and Amide-Linked Basket-Handle and Picket-Fence Iron Porphyrins

Doris Lexa,[1a] Michel Momenteau,[1b] Philippe Rentien,[1a] Gérard Rytz,[1a,c] Jean-Michel Savéant,*[1a] and Feng Xu[1a]

Contribution from the Laboratoire d'Electrochimie de l'Université de Paris 7, 75251 Paris Cedex 05, France, and the Institut Curie, Section de Biologie, Unité INSERM 219, Centre Universitaire, 91405 Orsay, France. *Received October 11, 1983*

Abstract: The presence of basket-handle chains or a picket-fence structure exerts a pronounced influence on the redox and coordination chemistry of iron porphyrins. The electrochemical behavior of four different ether-linked basket-handle, three different amide-linked basket-handle, and one amide-linked picket-fence iron porphyrins was investigated in comparison with 5,10,15,20-tetra-*o*-anisylporphyrin in the first series and 5,10,15,20-tetraphenylporphyrin in the second. Large effects of the superstructures appear in the thermodynamics of the three successive $Fe^{III} \rightarrow Fe^{II} \rightarrow Fe^{I} \rightarrow Fe^{I}$· reduction steps and the Cl^-/DMF substitution reaction at Fe^{II}. The kinetics of the latter reaction also varies significantly in the series. All four reactions are thermodynamically unfavored by the ether-linked chains while the amide-linked structures produce completely opposite effects. Changes as large as 4–5 orders of magnitude result. Steric hindrance to solvation of the negatively charged complexes appears as the predominant effect of the ether-linked structures. Steric interactions between the chains and the axial ligands also manifest themselves in the thermodynamics of the $[Fe^{II}DMF]/[Fe^{I}]^-$ electron-transfer reaction as well as the Cl^-/DMF substitution process at Fe^{II}. These effects also exist in the amide-linked series. They are, however, largely overcompensated by a specific effect of the NHCO groups involving hydrogen bonding and/or dipole–charge interactions resulting in a strong stabilization of the negatively charged species. In both series, steric interactions between the chains and the axial ligands appear to be responsible for the large variations in the ligand exchange and electron-transfer reactions when passing from flexible to more rigid chains.

In an effort to mimic and understand the dioxygen transport and activation properties of hemoproteins, several types of superstructured iron porphyrins have been synthesized and characterized during the last 10 years. These "picket-fence",[2] "capped",[3] "cyclophane",[4] "pocket",[5] "crowned",[6] "strapped",[7] and "basket-handle"[8] iron porphyrins were originally devised to protect

(1) (a) Université de Paris 7. (b) Institut Curie. (c) Present address: 180-160 Ciba Gegy A-G Forschun G-S Zentrum K.A. Postfach-CH-1701, Fribourg, Suisse.

(2) (a) Collman, J. P.; Gagne, R. R.; Halbert, T. R.; Marchon, J. C.; Reed, C. A. *J. Am. Chem. Soc.* **1973**, *95*, 7868. (b) Collman, J. P.; Gagne, R. R.; Reed, C. A.; Halbert, T. R.; Lang, G.; Robinson, W. T. *Ibid.* **1975**, *97*, 1427. (c) Collman, J. P. *Acc. Chem. Res.* **1977**, *10*, 265. (d) Collman, J. P.; Brauman, J. I.; Doxsee, K. M.; Halbert, T. R.; Suslick, K. S. *Proc. Natl. Acad. Sci. U.S.A.* **1978**, *75*, 564. (e) Jameson, G. B.; Molinaro, F. S.; Ibers, J. A.; Collman, J. P.; Brauman, J. I.; Rose, E.; Suslick, K. S. *J. Am. Chem. Soc.* **1980**, *102*, 3224. (f) Collman, J. P.; Groh, S. E. *Ibid.* **1982**, *104*, 1391.

(3) (a) Almog, J.; Baldwin, J. E.; Dyer, R. L.; Peters, M. K. *J. Am. Chem. Soc.* **1975**, *97*, 226. (b) Almog, J.; Baldwin, J. E.; Grossley, M. J.; Debernardis, J. F.; Dyer, R. L.; Huff, J. R.; Peters, M. K. *Tetrahedron* **1981**, *37*, 3589. (c) Baldwin, J. E.; Crossley, M. J.; Klox, T.; O'Rear, E. A.; Peters, M. K. *Ibid.* **1982**, *38*, 27. (d) Budge, J. R.; Ellis, P. E., Jr.; Jones, R. D.; Linard, I. E.; Szymanski, T.; Basolo, F.; Baldwin, J. E.; Dyer, R. H. *J. Am. Chem. Soc.* **1979**, *101*, 4762.

(4) (a) Diekmann, H.; Chang, C. K.; Traylor, T. G. *J. Am. Chem. Soc.* **1971**, *93*, 4068. (b) Traylor, T. G.; Campbell, D.; Tsuchiya, S. *Ibid.* **1979**, *101*, 4748. (c) Traylor, T. G.; Campbell, D.; Tsuchiya, S.; Stynes, D. V. *Ibid.* **1980**, *102*, 5939. (d) Traylor, T. G. *Acc. Chem. Res.* **1981**, *14*, 102. (e) Traylor, T. G.; Traylor, P. S. *Annu. Rev. Biophys. Bioeng.* **1982**, *11*, 105.

(5) (a) Collman, J. P.; Brauman, J. I.; Collins, T. J.; Iverson, B. L.; Sessler, J. L. *J. Am. Chem. Soc.* **1981**, *103*, 2450.

0002-7863/84/1506-4755$01.50/0

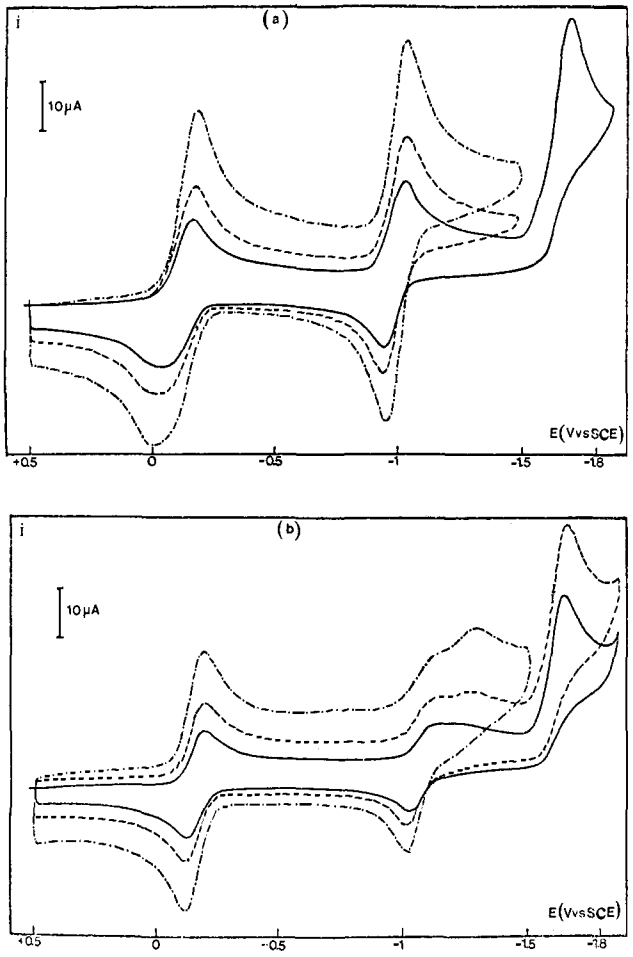

Figure 1. Cyclic voltammetry of $ClFe^{III}TPP$ (1 mM) in DMF + 0.1 M $LiClO_4$: (a) without addition of Cl^-; (b) $[Cl^-] = 1$ M (sweep rate = 0.1, 0.2, and 0.5 $V\ s^{-1}$).

the $Fe^{II}O_2$ complexes against oxidation leading to the μ-oxo dimer[2c,4d,e] as well as to sterically favor the formation of a pentacoordinated complex with an external base that appears as a necessary requirement for good oxygen binding.

Several factors affecting the thermodynamics and kinetics of the dioxygen and carbon monoxide binding to these protected hemes have been investigated and discussed (see ref 2c, 4d,e, 8c,e, 9, and 10 and references cited therein). Among them, two observations are of particular relevance to the following discussion. (i) Solvation is regarded as an important factor responsible for lower O_2 and CO affinities of the unprotected hemes as compared to those of the protected picket-fence porphyrins.[9b,11] (ii) Comparing ether-linked to amide-linked basket-handle porphyrins, both involving a pending pyridine ligand on one side, it has been observed that the dioxygen adduct is stabilized by distal polar interactions in the second case as compared to the first.[8c] Proton NMR evidence has been observed for the formation of H bonds between the H atom of the NHCO groups and dioxygen.[10]

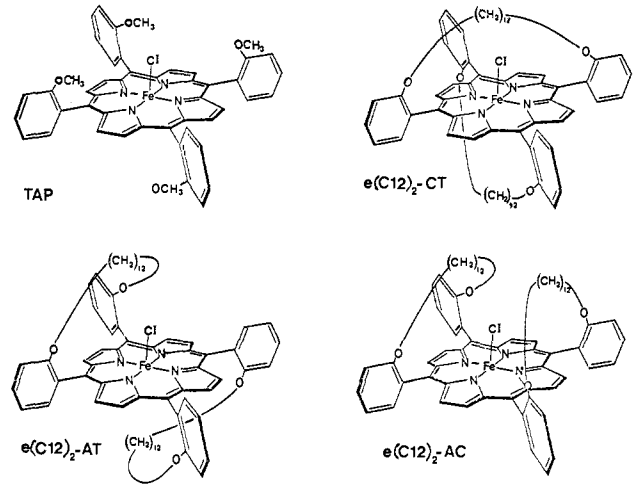

Figure 2. Iron(III) chloride–ether-linked C12 basket-handle porphyrins and tetra-*o*-anisylporphyrin.

Comparing the electrochemical characteristics of several basket-handle and picket-fence iron porphyrins to those of the corresponding, unprotected complexes under the same conditions, we have observed that their redox and coordination chemistry is dramatically affected by the presence of the protecting structures. Starting from the Fe^{III} chloro complex, three successive electrochemical reactions were investigated corresponding to the successive formation of Fe^{II} and Fe^{I} complexes and of the ring anion radical. We first describe the results of this investigation in the case of ether-linked basket-handle tetraphenylporphyrins. Their rationalization provides evidence that the presence of the ether-linked protecting chains causes steric hindrance against solvation of the negatively charged species and steric destabilization of the axial ligands. When the ether linkages are replaced by amide linkages, the observed effects are opposite, showing the existence of strong polar interactions with the NHCO groups. These are able to cause differences as large as 5 orders of magnitude in terms of equilibrium constants.

These electrochemical results and their interpretation contribute to understand to what extent and how supermolecular structures can influence the redox and coordination chemistry of iron porphyrins. This knowledge is of particular interest in the case of amide-linked structures that are reminiscent of the presence of NHCO groups in the metalloprotein. It may also prove useful in the design and analysis of catalytic cycles based upon changes of the oxidation state of the central metal atom.

Figure 1a recalls the general features of the three successive reduction steps of a $Fe^{III}Cl$ porphyrin complex. They show the cyclic voltammograms obtained for the reduction of $Fe^{III}TPPCl$[12] in DMF[12] at a glassy carbon electrode with $LiClO_4$ as supporting electrolyte. Going from positive to negative potentials, three successive reduction stages are identified. As results from earlier work,[13] they correspond to the following reactions.

(6) Chang, C. K. *J. Am. Chem. Soc.* **1977**, *99*, 2819.
(7) (a) Battersby, A. R.; Buckley, D. G.; Hartley, S. G.; Turnbull, M. D. *J. Chem. Soc., Chem. Commun.* **1976**, 879. (b) Baldwin, J. E.; Klose, T.; Peters, M. *Ibid.* **1976**, 881. (c) Battersby, A. R.; Hartley, S. G.; Turnbull, M. D. *Tetrahedron Lett.* **1978**, 3169. (d) Battersby, A. R.; Hamilton, A. D. *J. Chem. Soc., Chem. Commun.* **1980**, 117.
(8) (a) Momenteau, M.; Loock, B.; Mispelter, J.; Bisagni, E. *Nouv. J. Chim.* **1979**, *3*, 77. (b) Momenteau, M.; Loock, B. *J. Mol. Catal.* **1980**, *7*, 315. (c) Momenteau, M.; Lavalette, D. *J. Chem. Soc., Chem. Commun.* **1982**, 341. (d) Momenteau, M.; Mispelter, J.; Loock, B.; Bisagni, E. *J. Chem. Soc., Perkin Trans. 1* **1983**, 189. (e) Momenteau, M.; Loock, B.; Lavalette, D.; Tetreau, C.; Mispelter, J. *J. Chem. Soc., Chem. Commun.* **1983**, 962. (f) Momenteau, M.; Loock, B.; Mispelter, J., submitted for publication.
(9) (a) Collman, J. P.; Brauman, J. I.; Doxsee, K. M.; Sessler, J. L.; Morris, R. M.; Gibson, Q. H. *Inorg. Chem.* **1983**, *22*, 1427. (b) Collman, J. P.; Brauman, J. I.; Iverson, B. L.; Sessler, J. L.; Morris, R. M.; Gibson, Q. H. *J. Am. Chem. Soc.* **1983**, *105*, 3052.
(10) Mispelter, J.; Momenteau, M.; Lavalette, D.; Lhoste, J. M. *J. Am. Chem. Soc.* **1983**, *105*, 5165.
(11) (a) Collman, J. P.; Brauman, J. I.; Doxsee, K. M.; Halbert, R. T.; Hayes, S. E.; Suslick, K. S. *J. Am. Chem. Soc.* **1978**, *100*, 2761. (b) Collman, J. P.; Brauman, J. I.; Halbert, T. R.; Suslick, K. S. *Proc. Natl. Acad. Sci. U.S.A.* **1979**, *76*, 6035.

(12) Abbreviations: DMF, dimethylformamide; TPP, 5,10,15,20-tetraphenylporphyrin; TAP, 5,10,15,20-tetra-*o*-anisylporphyrin; basket-handle porphyrins (BHP). The nomenclature of these compounds has been already published in ref 8d. To facilitate the reading of this paper, we use the following notations: e(C12)$_2$-AT, adjacent-trans isomer of the basket-handle porphyrin bearing two aliphatic twelve carbon chains, linked each by an oxygen atom to the ortho position of the phenyl rings of TPP; e(C12)$_2$-AC, adjacent-cis isomer of the same porphyrin; e(C12)$_2$-CT, cross-trans isomer of the same porphyrin (see Figure 3); e[di(C4)Ph]$_2$-CT, cis-trans isomer of the basket-handle porphyrin bearing two $-(CH_2)_4C_6H_4(CH_2)_4-$ chains each linked by an oxygen atom to one ortho positions of the phenyl rings of TPP (see Figure 10).

Table I. Electrochemical Characteristics of the Reduction of $Fe^{III}Cl$ Ether-Linked C12 Basket-Handle Porphyrins[12] As Compared to $Fe^{III}Cl$ 5,10,15,20-Tetra-*o*-anisylporphyrin

	reaction 1				reaction 2	reaction 3
	$E_{[Fe^{III}Cl]/[Fe^{II}Cl]^-}$[a,e]	K_A^{II}[b]	k_a^{II}[c]	k_d^{II}[d]	$E^\circ_{[Fe^{II}/DMF]/[Fe^I]^-}$[a,e]	$E^\circ_{[Fe^I]^-/[Fe^{I\cdot}]^{2-}}$[a,f]
TAP	−0.281	31	2.5×10^3	0.8×10^2	−1.058	−1.767
e(C12)$_2$-AC	−0.365 (84)	3.6	1.3×10^5	3.6×10^4	−1.098 (40)	−1.842 (75)
e(C12)$_2$-AT	−0.398 (117)	0.34	5.3×10^4	1.6×10^5	−1.093 (35)	−1.862 (95)
e(C12)$_2$-CT	−0.391 (110)	0.65	1.9×10^3	2.9×10^3	−1.125 (67)	−1.947 (180)
e[di(C4)Ph]$_2$-CT	−0.379 (98)	0.096	2.9×10^2	3.0×10^3	−1.078 (29)	−1.938 (171)

[a] Standard potential in V vs. NaCl SCE; the value of ΔE° in mV referred to TAP is given in parentheses. [b] Association equilibrium constant of Fe^{II} with Cl^- in M^{-1}. [c] Association rate constant of Fe^{II} with Cl^-, in $M^{-1}\ s^{-1}$. [d] Dissociation rate constant in s^{-1}. [e] Potentials measured in DMF with $LiClO_4$, 0.1 M. [f] Potentials measured in DMF with NBu_4BF_4, 0.1 M (which contains less water than $LiClO_4$).

The first wave features the reduction of the Fe^{III} complex to the Fe^{II} complex. The anodic wave is composite involving two overlapping waves corresponding to the oxidation of the $[Fe^{II}Cl]^-$ complex (the most anodic) and the $[Fe^{II}DMF]$ complex (the less anodic), respectively. The reactions occurring at this wave can be summarized by the following "square" scheme shown in eq 1.[14] The second reversible couple corresponds to reaction 2.[13a,d,f,14c,16] The third wave, the so-called "ring wave", which is reversible in dry DMF (H_2O < ca. 0.05%) corresponds to the redox couple shown in eq 3.[17] When the water content is higher (ca. 2%, Figure

$$\begin{array}{ccc} [Fe^{III}Cl] + 2\,DMF & \rightleftharpoons & [Fe^{III}(DMF)_2]^+ + Cl^- \quad (C_{III}) \\ +e \downarrow\uparrow & & \uparrow\downarrow +e\ (DMF) \\ [Fe^{II}Cl]^- + DMF & \rightleftharpoons & [Fe^{II}DMF] + Cl^- \quad (C_{II}) \end{array} \qquad (1)$$

$$K_A^{II} = [Fe^{II}Cl]^-/[Fe^{II}DMF][Cl^-]$$

$$[Fe^{II}DMF] + 1e \rightleftarrows [Fe^I]^- + DMF \qquad (2)$$

$$[Fe^I]^- + 1e \rightleftarrows [Fe^{I\cdot}]^{2-} \qquad (3)$$

1a), this wave exhibits a two-electron height and becomes irreversible, most likely featuring an irreversible 2e + $2H^+$ reduction of the ring, along and ECEC-type mechanisms by analogy to what occurs in the reduction of aromatic hydrocarbons, such as anthracene, in DMF upon addition of proton donors.[18]

Ether-Linked Basket-Handle Iron Porphyrins

Results. The formulas of the basket-handle porphyrins we investigated are shown in Figure 2. They involve two 12-carbon aliphatic linear chains, each attached through ether linkages to the ortho positions of two phenyl groups of the 5,10,15,20-tetraphenylporphyrin complex. Three isomers can thus be obtained: cross-trans (CT), adjacent-trans (AT), and adjacent-cis (AC). Linear chains involving twelve carbon atoms and two terminal oxygen atoms were selected rather than shorter straps with the aim of avoiding enforcement of nonplanarity of the porphyrin ring. In order to discriminate steric effects of the chains, in which we were mostly interested, from possible electron-donating effects[13f] of the four ether groups, we systematically compared the electrochemical behavior of the basket-handle porphyrins to that of 5,10,15,20-tetra-*o*-anisyl porphyrin (TAP)[12] (Figure 2)[19] rather than to TPP itself. The electron-donating effect is indeed anticipated to be smaller, or at maximum equal, in the basket-handle complexes than in TAP.

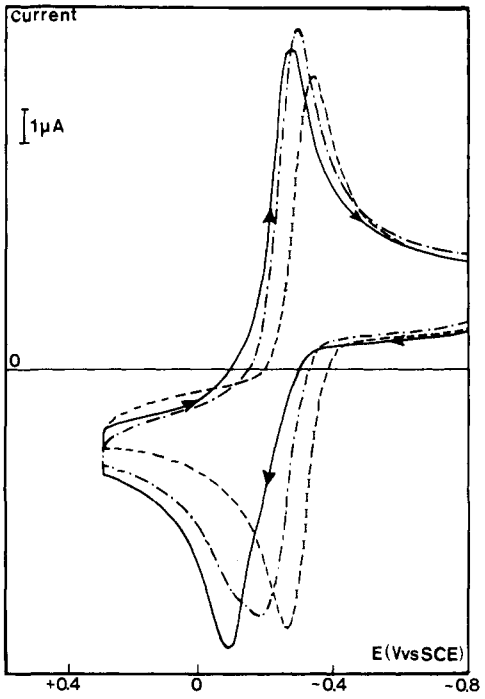

Figure 3. Cyclic voltammetry of $ClFe^{III}TAP$ (1.17 mM) in DMF + 0.1 M $LiClO_4$ at a glassy carbon electrode as a function of LiCl concentration [sweep rate = 0.1 V s^{-1}; starting potential = −0.8 V; LiCl concentration 0 (—), 0.96 10^{-2} M (−·−), 0.186 M (- - -)].

Electrochemistry of Iron CT, AT, and AC Basket-Handle Porphyrins As Compared to That of Iron Tetra-*o*-anisylporphyrin in DMF. Cyclic voltammetry in DMF shows that reactions 2 and 3 are reversible for the four complexes under the same conditions as for TPP. The potential differences between the anodic and cathodic peaks are slightly larger (70–80 mV) than the value corresponding to a purely Nernstian wave (58 mV). The standard

(13) (a) Lexa, D.; Momenteau, M.; Mispelter, J. *Biochim. Biophys. Acta* **1974**, *338*, 151. (b) Davis, D. G. In: "The Porphyrins"; Dolphin, D., Ed.; Academic Press: New York, 1978; Vol. 5, pp 127–152. (c) Bottomley, L. A.; Kadish, K. M. *Inorg. Chem.* **1981**, *20*, 1348. (d) Reed, C. A. In: "Biological Redox Components"; Kadish, K. M., Ed.; American Chemical Society: Washington, DC, 1982; *Adv. Chem. Ser. No.* 201, Chapter 15, pp 333–356. (e) Kadish, K. M.; Rhodes, R. K. *Inorg. Chem.* **1983**, *22*, 1090. (f) Kadish, K. M. In: "Physical Bioinorganic Chemistry Series. Iron Porphyrins"; Lever, A. P. B., Gray, H. B., Eds.; Addison-Wesley: Reading, MA, 1982; Part II, Chapter 4, pp 161–249. (g) Lexa, D.; Mispelter, J.; Savéant, J. M. *J. Am. Chem. Soc.* **1981**, *103*, 6806.

(14) (a) Qualitative evidence for the correctness of this reaction mechanism has been given.[13c,e,f] A quantitative analysis of the reaction mechanism has been carried out in this laboratory and will be published elsewhere.[14b] (b) Lexa, D.; Rentien, P.; Savéant, J. M.; Xu, F., manuscript in preparation. (c) It has been shown that $Fe^{II}TPP$ coordinates only one molecule of DMF axially in benzene[15] and in dichloromethane[13c] with small association constants, 6.2 and 2 M^{-1}, respectively. It can thus be inferred that there is also only one coordinated DMF molecule in pure DMF also.

(15) Brault, D.; Rougee, M. *Biochemistry* **1974**, *13*, 4591.

(16) (a) A recent careful discussion[13d] of electrochemical, spectral, and X-ray data concluded that among the iron(I) and iron(II) anion radical resonance forms of the complex formed upon one-electron reduction of the Fe^{II} complex, the former is predominant. (b) Provided that the chloride ions are not introduced into the solution in addition to the stoichiometric amount involved in the starting ferric chloro complex, the Fe^{II} chloro complex does not interfere with the redox reaction.[14b]

(17) The spectral and X-ray characteristics of the reduced complex indicate that it is best regarded as a resonance hybrid of the iron(I) anion radical and the iron(II) diradical dianion.[13d]

(18) Amatore, C.; Gareil, M.; Savéant, J. M. *J. Electroanal. Chem.* **1983**, *147*, 1 and references cited therein.

(19) The compound we actually studied was a mixture of the four $\alpha\alpha\alpha\alpha$, $\alpha\alpha\alpha\beta$, $\alpha\alpha\beta\beta$, and $\alpha\beta\alpha\beta$ atropo isomers rather than only the $\alpha\alpha\alpha\alpha$ isomer shown in Figure 2. The observed electrochemical properties are thus an average of those for each of the four isomers that are expected to be very close to one another.

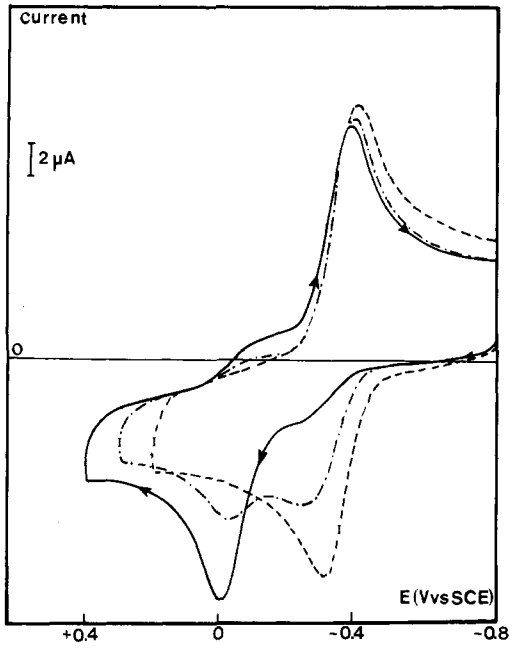

Figure 4. Cyclic voltammetry of $ClFe^{III}e(C12)_2$-AT (0.84 mM) in DMF + 0.1 M $LiClO_4$ at a glassy carbon electrode as a function of LiCl concentration [starting potential = −0.8 V; sweep rate = 0.4 V s^{-1}; LiCl concentration, 0 (–), 0.38 10^{-1} M (–·–), 0.427 M (- - -)].

potentials of the two reactions were derived from the midpoint between the anodic and cathodic peaks. It was noticed that the values thus obtained (Table I) are practically insensitive to the nature of the supporting electrolyte cation from NBu_4^+ to Li^+. For the two reactions, there are significant differences between the basket-handle porphyrins and TAP.

As mentioned earlier, Cl^-/DMF ligand exchange reactions interfere in the Fe^{III}/Fe^{II} wave in addition to the Fe^{III}/Fe^{II} electron-transfer reactions. Starting with $LiClO_4$ as the supporting electrolyte, LiCl was thus added to the solution and its concentration systematically varied in order to analyze the overall redox process. The Fe^{III} complexes have a large affinity for chloride ions.[13c,14b] Step C_{III} in reaction 1 can therefore be regarded as irreversible from right to left in the following discussion. It follows that the most convenient way of looking at the role of the Cl^-/DMF exchange is to start from the Fe^{II} oxidation state, first to oxidize and then to reduce. Typical voltammograms obtained under these conditions for TAP and $e(C12)_2$-AT[12] are shown in Figures 3 and 4. The variations observed upon addition of Cl^- at a given sweep rate are given in Figures 3 and 4. Two waves are visible on the anodic scan, and one wave is visible on the cathodic scan. The first wave on the anodic scan features the oxidation of the $[Fe^{II}Cl]^-$ complex, which is easier to oxidize than the $[Fe^{II}DMF]$ complex, the oxidation of which corresponds to the second anodic wave. Both oxidation processes lead rapidly and irreversibly to the stable $[Fe^{III}Cl]$ complex. This is reduced in a single wave on the cathodic scan.

The anodic pattern thus indicates the occurrence of a "CE" (chemical–electrochemical) mechanism.[20a] Such CE mechanisms associated with ligand exchange reactions are rather common in coordination electrochemistry.[20b] Here, the chemical reaction is the Cl^-/DMF ligand exchange at the Fe^{II} oxidation level (eq C_{II}). The height of the first anodic wave relative to the height of a one-electron diffusion-controlled process thus reflects the thermodynamics and kinetics of reaction C_{II}. It primarily corresponds to the amount of the most oxidizable complex $[Fe^{II}Cl]^-$ present at equilibrium, but there is, in addition, a kinetic contribution to the current resulting from the dynamic conversion of the DMF complex into the chloro complex within the time scale of the experiment. This kinetic contribution is predicted to decrease when the sweep rate is raised. This is indeed what is observed: when the sweep rate is raised, the first wave decreases at the expense of the second. The addition of increasing amounts of Cl^- raises both the amount of $[Fe^{II}Cl]^-$ at equilibrium and the kinetic component as shown in Figures 3 and 4. It thus appears qualitatively that both the thermodynamics and kinetics of reaction C_{II} are different when passing from the TAP to the $e(C12)_2$-AT porphyrin. The same remark holds for the two other isomers.

Determination of the rate constants of reaction C_{II} can be obtained from the cyclic voltammetric data by using the available theory for the CE mechanisms.[20a] However, for this, the equilibrium constant must be know independently. This was obtained by spectrometric titration of the Fe^{II} complexes by chloride ions. A thin layer cell containing a platinum grid as a working electrode was used to generate the Fe^{II} complex at an appropriate potential selected from the results of cyclic voltammetry. Addition of Cl^- results in modifications of the Q bands. However, these are not large enough to allow a precise titration. The variations observed in the Soret region are more important (Table II) and were therefore used for the titration. The values of the association equilibrium constant for reaction C_{II}, K_A^{II}, obtained by this method with the four porphyrins are listed in Table I. Significant differences are again observed.

Once K_A^{II} is known, it is possible to derive the chloride association and dissociation rate constants, k_a^{II} and k_d^{II}, from the height of the first anodic kinetic wave.[20a] The results are given in Table I.

At high concentrations of chloride and low sweep rates (Figures 1, 3, and 4) the cyclic voltammetry pattern corresponding to reaction 1 shows only one anodic wave that forms a reversible system with the cathodic wave. Complete mobility of equilibrium C_{II} is then achieved in the time scale of the experiment: depletion of the $[Fe^{II}Cl]^-$ complex through oxidation at the electrode surface is immediately compensated by the fast equilibration of reaction C_{II}.[21a] Under these conditions, the apparent standard potential,

Table II. Characteristics of the Soret Band of the $[Fe^{II}DMF]$ and $[Fe^{II}Cl]^-$ Complex of TAP and Ether-Linked Basket-Handle Porphyrins[12] in DMF + 0.1 M $LiClO_4$

	λ_{max}, nm				
	TAP	$e(C12)_2$-AC	$e(C12)_2$-AT	$e(C12)_2$-CT	$e[di(C4)Ph]_2$-CT
$[Fe^{II}DMF]$	431	431	432	432	432
$[Fe^{II}Cl]^-$	441	443	443	444	*a*

[a] LiCl is not enough soluble in DMF at 20 °C to obtain quantitatively the $[Fe^{II}Cl]^-$ complex in a way that gives an accurate λ_{max}.

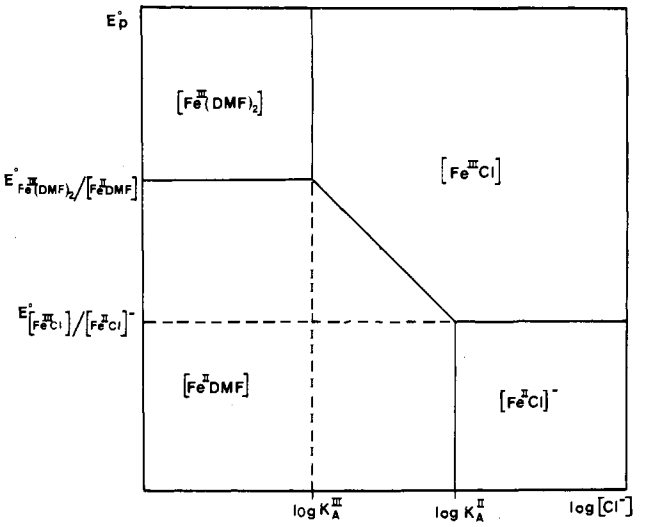

Figure 5. Apparent standard potential vs. chloride concentration diagrams showing the range of thermodynamical stabilities of the participants of reaction 1. The oblique descending line has a slope of (RT/F) ln 10.

(20) (a) Savéant, J. M.; Vianello, E. *Electrochim. Acta* **1963**, *8*, 905. (b) Lexa, D.; Savéant, J. M. *Acc. Chem. Res.* **1983**, *16*, 235.

Table III. Characteristics of Reactions 2 and 3 for TAP and e(C12)$_2$-CT in Benzonitrile

	$E^\circ_{[Fe^{II}]/[Fe^{I}]^-}$[a]	$E^\circ_{[Fe^{I}]^-/[Fe^{I\cdot}]^{2-}}$[a]
TAP	−1.107	−1.734
e(C12)$_2$-CT	−1.237 (130)	−1.925 (191)

[a] In V vs. NaCl SCE. The difference between the standard potential of TAP and e(C12)$_2$-CT is given in mV in parentheses.

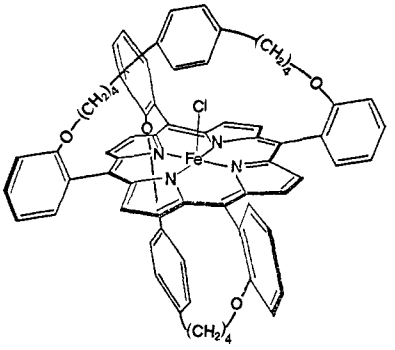

Figure 6. Structure of the e[di(C4)Ph]$_2$-CT basket-handle iron complex.

E°_{ap}, defined as the midpoint between these anodic and cathodic peaks is not necessarily equal to $E^\circ_{[Fe^{III}Cl]/[Fe^{II}Cl]}$ and may depend upon the Cl^- concentration according to the thermodynamic diagram shown in Figure 5. In the present study, E°_{ap} was located on the descending oblique line of the diagram. It is then given by[20a]

$$E^\circ_{ap} = E^\circ_{[Fe^{III}Cl]/[Fe^{II}]^-} - (RT/F) \ln \{K_A^{II}[Cl^-]/(1 + K_A^{II}[Cl^-])\}$$

Since we now know K_A^{II}, we can derive $E^\circ_{[Fe^{III}Cl]/[Fe^{II}Cl]^-}$ from E°_{ap} in the experiments where reaction 1 gives rise to a single reversible wave. The results are listed in Table I.

Additional Experiments. In order to gain further insight into the role of solvation, we compared the electrochemical behavior of the TAP and e(C12)$_2$-CT[12] complexes in benzonitrile. As expected, chloride association to Fe^{II} appears, in the framework of reaction 1, larger than that in DMF. Benzonitrile is indeed anticipated to be a poorer ligand than DMF. Two reversible waves corresponding to reactions 2 and 3 were again observed. The ensuing values of the standard potentials are given in Table III.

The rationalizations of the various effects of the basket-handle chains presented in the discussion section were originally based upon the comparison between the TAP complex and the three e(C12) basket-handle isomeric complexes. On the basis of these conclusions, we then tried to predict semiquantitatively what the effects should be for the three successive reactions in the case of the e[di(C4)Ph]$_2$-CT[12] complex, the structure of which is shown in Figure 6. The electrochemical behavior in cyclic voltammetry and thin-layer spectroelectrochemistry is qualitatively the same as that for the four other complexes. The Soret band characteristics are given in Table II whereas the values of the standard potentials of the three waves and the equilibrium and rate constants of reaction C_{II} are listed in Table I.

Discussion. The most striking feature of the results described above is the parallelism of the variations of three thermodynamical parameters characterizing reactions 1–3 when passing from the TAP complex to the basket-handle complexes as a whole: K_A^{II} decreases, $E^\circ_{[Fe^{II}DMF]/[Fe^{I}]^-}$ decreases and $E^\circ_{[Fe^{I}]^-/[Fe^{I\cdot}]^{2-}}$ decreases.

(21) (a) For TPP it was found[14b] that K_A^{II} = 56 M^-, $E^\circ_{[Fe^{II}DMF]/[Fe^{I}]^-}$ = −0.984 V, and $E^\circ_{[Fe^{I}]^-/[Fe^{I\cdot}]^{2-}}$ = −1.68 V, clearly showing the effect of electron donation of the four methoxy groups in TAP. (b) On one hand, CH_3O is a better electron-donating group than R-CH_2-O, and on the other, the restricted rotation around the porphyrin ring–phenyl bond in the case of basket-handle porphyrins may forbid any conjugation between the phenyl groups and the porphyrin ring, thus decreasing the electron-donating effect of the ether groups as compared to what happens with TAP.

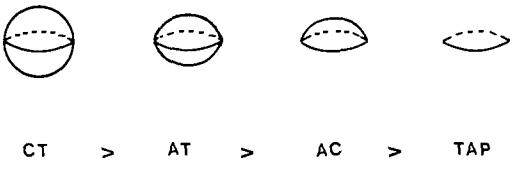

Figure 7. Schematic picture of steric hindrance to solvation.

The three corresponding elementary reactions have in common that the charge of the reactants becomes one unit more negative from the left-hand side to the right-hand side. It thus appears the the ether-linked basket-handle structure destabilizes the negatively charged complexes as compared to TAP.

Electron donation to the porphyrin ring by the ether substituents destabilizes the negatively charged species leading to a variation of the three parameters in the same direction.[21a] We, however, note that electron donation is larger, or at least equal, in TAP than in the basket-handle complexes.[21b] In this context, the variations of the three parameters should therefore be in the opposite direction or at most negligible. We thus conclude that the observed variations are not due to a substituent electronic effect on the porphyrin π electrons through the phenyl groups. For the same reasons, they are not due either to the through-space electronic effects of the ether groups that would exist in TAP as well as in the basket-handle derivatives.

We are thus led to relate the observed effect to differences in solvation. The chains sterically hinder the solvation of the negatively charged species, thus destabilizing $[Fe^{II}Cl^-]$ toward $[Fe^{II}DMF]$, $[Fe^{I}]^-$ toward $[Fe^{II}DMF]$, and $[Fe^{I\cdot}]^{2-}$ toward $[Fe^{I}]^-$ as compared to what happens with TAP. This falls in line with the observation that the potential shifts for reaction 3 are significantly larger than those for reaction 2, in accordance with the fact that the charge passes from 1− to 2− in the former case and from 0 to 1− in the latter (in a Born-type model, the free energy of solvation varies with the square of the charge).

A first conclusion is thus that steric hindrance to solvation of the charged complexes appears as a major factor in the influence of the chains on the electrochemistry of basket-handle iron porphyrins.

Let us now look at the data of Table I in a more detailed manner, comparing not only TAP to the basket-handle complexes as a whole but also considering the differences between the three e(C12) isomers. It immediately appears that the orders found for reactions C_{II}, 2, and 3 are different: K_A^{II} decreases in the order TAP > e(C12)$_2$-AC > e(C12)$_2$-CT ≥ e(C12)$_2$-AT; $E^\circ_{[Fe^{II}DMF]/[Fe^{I}]^-}$ in the order TAP > e(C12)$_2$-AT ≥ e(C12)$_2$-AC > e(C12)$_2$-CT, $E^\circ_{[Fe^{I}]^-/[Fe^{I\cdot}]^-}$ in the order TAP > e(C12)$_2$-AC > e(C12)$_2$-AT > e(C12)$_2$-CT.

Since both the $[Fe^{I}]^-$ and $[Fe^{I\cdot}]^{2-}$ complexes have no axial ligand, reaction 3 is the most representative of the effect of steric hindrance against solvation discussed above. As shown by proton NMR data,[8a] the chains are more flexible in the AT and AC isomers than in the CT isomer (more for the AT than for the AC isomer). They can thus be more compressed by the solvent on the porphyrin ring in the former case than in the latter. The equivalent radii of solvation then lie in the order e(C12)$_2$-CT > e(C12)$_2$-AT > e(C12)$_2$-AC > TAP, as pictured in Figure 7, taking also into account that the AC isomer is protected only on one face.

The difference in $E^\circ_{[Fe^{I}]^-/[Fe^{I\cdot}]^{2-}}$ between TAP and e(C12)$_2$-CT is of the same order of magnitude in benzonitrile (191 mV) and in DMF (180 mV). The solvation free energies of the negatively charged complexes thus appear to be of the same order of magnitude in both solvents. DMF has a larger dielectric constant (36.5) than benzonitrile (25.6) but has less propensity to solvate anions.

In reaction 2, the negatively charged $[Fe^{I}]^-$ complex is destabilized by steric hindrance to solvation in the same order as above. However, the axial DMF ligation of the $[Fe^{II}DMF]$ complex may also be weakened by the steric interaction of the DMF ligand with the chains. This effect would be the largest for the AT isomer due to the flexibility of the chains as compared to that of the more rigid CT isomer and to that of the AC isomer where steric in-

teractions occur only on one face. Destabilization of the $Fe^{II}DMF$ complex contributes to render the standard potential less negative. It is thus understandable that the $E°_{[Fe^{II}DMF]/[Fe^{I}]^-}$ values for the AT and AC complexes are inverted as compared to the $E°_{[Fe^{I}]^-/[Fe^{I}]^{2-}}$ values.

The difference in $E°_{[Fe^{II}]/[Fe^{I}]^-}$ between TAP and e(C12)$_2$-CT is larger in benzonitrile (130 mV) than in DMF (70 mV) in spite of the observation that solvation of the same negative complex appears to be roughly the same as noted above. This results from the fact that benzonitrile is a much poorer ligand of Fe^{II} than DMF: since benzonitrile practically does not coordinate with Fe^{II}, there is no steric destabilization of the Fe^{II} member of the Fe^{II}/Fe^{I} couple when passing from TAP to e(C12)$_2$-CT as it was the case with DMF.

As regards the equilibrium constant of reaction C_{II}, differences in solvation of the $[Fe^{II}Cl]^-$ complex still play a predominant role explaining the observed order of reactivity. The K_A^{II} value for the AT isomer is, however, of the same order of magnitude, even slightly smaller, as for the CT isomer while steric hindrance to solvation as revealed by the $E°_{[Fe^{I}]^-/[Fe^{I}]^{2-}}$ values is significantly larger in the latter case than in the former. It is visible on molecular models that the cavity dimensions in the CT isomer allow steric discrimination between the Cl and DMF ligations favoring the former complex against the latter. This effect is predicted to be much less in the AT isomer where compression of the flexible chains on the porphyrin ring will leave little opportunity for steric discrimination. The same is likely to be true for the AC isomer taking also into account the protection of only one face. In other words, the variations of K_A^{II} in the TAP, e(C12)$_2$-AT, e(C12)$_2$-AC series are essentially governed by steric hindrance to solvation whereas an additional factor, steric discrimination between DMF and Cl, interferes in the CT isomer leading to a larger K_A^{II} value than predicted on the sole basis of steric hindrance to solvation.[22]

We have presently no data allowing us to estimate the effects of the basket-handle chains on the stability of neutral complexes such as $[Fe^{III}Cl]$.[23] It is therefore difficult to rationalize the rather small variations of $E°_{[Fe^{III}Cl]/[Fe^{II}Cl]^-}$ in the AC–AT–CT series. It is however apparent that steric hindrance to solvation of the $[Fe^{II}Cl]^-$ complex still plays a major role in the negative shift observed when passing from TAP to any of the basket-handle isomers.

Regarding now the kinetic data for reaction C_{II} (Table II) two facts are strikingly apparent. First, the dissociation and association rate constants are of the same order of magnitude for TAP and for the e(C12)$_2$-CT complex. Secondly, the AC and AT isomers show both faster association and dissociation, by 1–2 orders of magnitude, than the CT isomer. The same two observations were also made for the same isomers of amide-linked C12 basket-handle porphyrins, although chloride association is here favored by the chains as compared to the unprotected complexes (vide infra). This looks very puzzling at first sight since one is inclined to reason that the existence of steric barriers should slow down the substitution processes. Such reasoning however implicitly assumes the occurrence of a direct, S_N2-type, Cl^-/DMF substitution process. The observation that the presence of the chains tends, conversely, to speed up the association and dissociation reactions

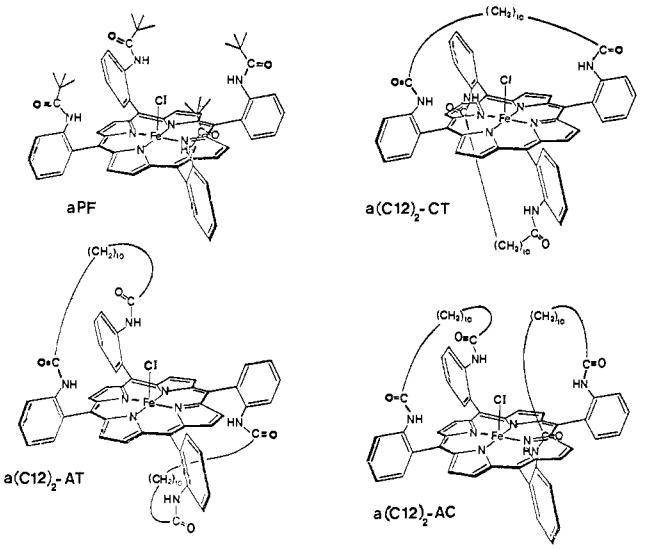

Figure 8. Iron(III) chloride–amido-linked C12 basket-handle porphyrins and picket-fence porphyrins.

points to the intermediacy of a four-coordinate complex leading to S_N1-like substitution processes. This does not mean however that steric hindrance of Cl^- and DMF attack of the four-coordinate intermediate by the chains cannot interfere simultaneously. In this context, the higher rate constants found with the AT and AC isomers as compared to those of the CT isomer can be interpreted as resulting from the larger flexibility of the chains inducing a more facile formation of the four-coordinate intermediate while steric hindrance to Cl^- and DMF attack does not vary significantly in the series.

In order to test the validity of the above interpretations, we undertook to predict semiquantitatively what the effects of the chains in a different basket-handle porphyrin, the e[di(C4)Ph]$_2$-CT derivative (Figure 6), should be and to see whether or not these predictions match the experimental observations.

Steric hindrance to solvation is expected to be of the same order of magnitude as for the e(C12)$_2$-CT porphyrin and so should be the value of $E°_{[Fe^{I}]^-/[Fe^{I}]^{2-}}$.

Coordination of a DMF molecule in axial position of the Fe^{II} complex is predicted to be destabilized by steric interaction with the freely rotating phenyl group present in the center of each chain. This should result in a less negative value of $E°_{[Fe^{II}DMF]/[Fe^{I}]^-}$ as compared to that of the e(C12)$_2$-CT porphyrin.

Steric interaction between the phenyl groups and the axial ligands should lead to little discrimination between Cl^- and DMF as in the e(C12)$_2$-AT case, conversely to what occurs in the e(C12)$_2$-CT case. Since steric hindrance to solvation is of the same order of magnitude as that in the e(C12)$_2$-CT case and is larger than that in the e(C12)$_2$-AT case, K_A^{II} should be smaller for e[di(C4)Ph]$_2$-CT than for e(C12)$_2$-CT and even e(C12)$_2$-AT.

Steric hindrance of Cl^- and DMF attack of the four-coordinate intermediate should slow down substitution at Fe^{II} as compared to the more flexible and less bulky AT and AC isomers.

Inspection of the data contained in the last row of Table I shows that all these predictions are in excellent agreement with the experimental results. Particularly striking is the comparison between the $E°_{[Fe^{I}]^-/[Fe^{I}]^{2-}}$ and $E°_{[Fe^{II}DMF]/[Fe^{I}]^-}$: e[di(C4)Ph]$_2$-CT shows the smallest shift of the latter parameter while e(C12)$_2$-CT shows the largest and e[di(C4)Ph]$_2$-CT shows the largest shift together with e(C12)$_2$-CT of the former parameter.

Amide-Linked Basket-Handle and Picket-Fence Iron Porphyrins

Results. As previously, most of the investigations were conducted in DMF as the solvent starting from the $Fe^{III}Cl$ complex. A few complementary experiments were carried out in benzonitrile and dimethylacetamide in order to investigate the possible role of the nature of the solvent in the observed effects.

(22) That steric hindrance to solvation decreases K_A^{II} by a factor of 10 in the case of the AC isomer (as compared to TAP) where only one face is protected implies that a substantial amount of the negative charge in the $[Fe^{II}Cl]^-$ complex is transferred from the chloride ion to the iron atom and the porphyrin ring.

(23) Are there local dielectric constant effects favoring ion pairing? Determination of K_A^{II} in poorly complexing solvents would be interesting in this connection. K_A^{III}, being too large, is difficult to measure spectrometrically even in DMF. We are currently developing an indirect electrochemical method for determining K_A^{III}.

(24) (a) "Handbook of Chemistry and Physics", 52nd ed.; CRC Press: Cleveland, OH, 1971; p D114. (b) Garreau, D.; Savéant, J. M. *J. Electroanal. Chem.* **1972**, *35*, 309. (c) Lexa, D.; Savéant, J. M.; Zickler, J. *J. Am. Chem. Soc.* **1977**, *99*, 2786. (d) Butler, J. N. "Ionic Equilibrium"; Addison-Wesley: Reading, MA, 1964; p 321.

(25) Zuman, P. "Substituent Effects in Organic Polarography"; Plenum Press: New York, 1967.

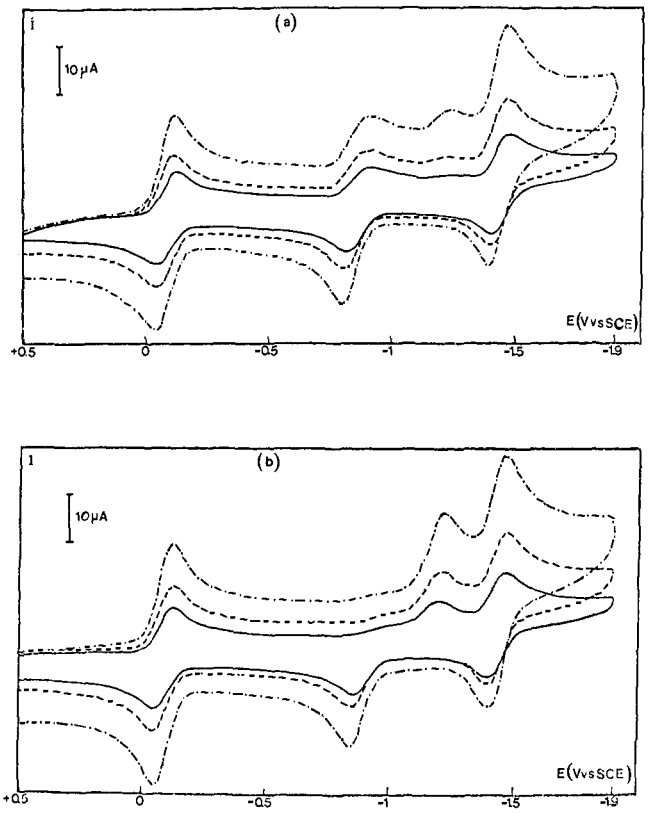

Figure 9. Cyclic voltammetry of $ClFe^{III}aPF$ (1 mM) in DMF + 0.1 M $LiClO_4$: (a) without addition of Cl^-. (b) $[Cl^-] = 1.1\ 10^{-2}$ M (sweep rate = 0.1, 0.2, and 0.5 V s^{-1}). The potential scale is referred to the NaCl SCE electrode.

Figure 8 shows the structure of the picket-fence and the three basket-handle iron porphyrins that were investigated. The chains in the basket-handle porphyrins have lengths almost identical with those of the ether-linked basket-handle complexes previously studied. Instead of twelve CH_2 and two O, we have now ten CH_2 and two NHCO. To facilitate the comparison, the three isomers of the amide-linked basket-handle complexes will be designated by $a(C12)_2$-CT (cross-trans attachement of the chains), $a-(C12)_2$-AT (adjacent-trans), and $a(C12)_2$-AC (adjacent-cis). The picket-fence complex will be noted as aPF.

When studying the ether-linked basket-handle complexes, we took TAP[12] as the reference unencumbered compound in order to free the comparison from electronic effects. Here, the reference compound is best selected as 5,10,15,20-tetraphenylporphyrin (TPP) since the Hammett constant for the –NHCOR substituents is very close to zero.[25]

Electrochemistry of $a(C12)_2$-CT, $a(C12)_2$-AT, $a(C12)_2$-AC, and aPF Iron Porphyrins As Compared to That of FeTPP in DMF. We start from the $[Fe^{III}Cl]$ complex in all cases. Figures 1 and 9 give a typical example of the compared cyclic voltammetric behaviors of a protected complex, aPF, and FeTPP at two chloride ion concentrations in DMF. In the first set of experiments (Figures 1a and 9a) no chloride ion was purposely added in the solution besides the amount in the porphyrin chloro complex. In the second set, 1 M Cl^- was added to the TPP solution (Figure 1b) and 10 mM Cl^- to the aPF solution (Figure 9b). Several qualitative features of the cyclic voltammograms are worth noting.

No particular care was taken for drying the DMF + 0.1 M $LiClO_4$ starting solution that contains about 0.2% water. Under these conditions the "ring wave", i.e., the most negative wave, is irreversible and shows a two-electron height in the case of TPP (Figure 1). As discussed earlier, the overall reaction involves reaction 3 as the first step followed by rapid protonation of $[Fe^{I}\cdot]^{2-}$ by residual water, further reduction, and further protonation. It is remarkable that with the same water concentration, the "ring wave" is a one-electron reversible wave in the case of the aPF complex, pointing to an increased stability of $[Fe^{I}\cdot]^{2-}$ toward protonation. The standard potentials can be derived from the aPF reversible "ring wave" and from the reversible one-electron "ring wave" of TPP obtained in drier solutions (less than 0.05% H_2O). It is observed that the former is less negative, by 240 mV, than the latter.

In the case of TPP with no Cl^- added, the first wave system, which corresponds to the "square scheme" sketched above, exhibits two overlapping anodic waves, featuring successively the oxidation of $[Fe^{II}Cl]^-$ (the more negative) and the oxidation of $[Fe^{II}DMF]$ (the less negative). As discussed in more detail elsewhere,[14b] a "CE" mechanism is involved in the oxidation process. The oxidation of $[Fe^{II}Cl]^-$ starts first. Depletion of $[Fe^{II}Cl]^-$ is partially compensated by the conversion of $[Fe^{II}DMF]$ according to reaction C_{II}. The relative height of the two anodic waves is thus a reflection of the thermodynamics and kinetics of reaction C_{II}. Upon addition of Cl^-, $[Fe^{II}Cl]^-$ tends to predominate and a single anodic wave is observed as shown in Figure 1b. It is however emphasized that the observation of a single wave does not necessarily mean that $[Fe^{II}Cl]^-$ is in excess over $[Fe^{II}DMF]$ at equilibrium. Even if the ratio $[Fe^{II}Cl]^-/[Fe^{II}DMF]$ is less than 1, a single wave may well be observed if the rate constants are large as compared to the diffusion rate. Under such conditions the apparent standard potential is a function of $K_A^{II}[Cl]^-$ where K_A^{II} is the equilibrium constant for reaction C_{II} as defined by

$$K_A^{II} = [Fe^{II}Cl]^-/[Fe^{II}DMF][Cl^-]$$

Another effect of the addition of Cl^- is seen in Figure 1b. The second cathodic wave, which was a single one-electron reversible wave in the absence of added Cl^-, is split into two successive waves. Reversibility then appears upon scan reversal at the level of the first cathodic wave while the second is irreversible. It is also noted that the height of the first cathodic wave relative to the second decreases when the sweep rate is raised. This again reflects a "CE" mechanism. Now, $[Fe^{II}DMF]$ is easier to reduce than $[Fe^{II}Cl]^-$, and the height of the first wave relative to the second is a function of the thermodynamics and kinetics of reaction C_{II} within the time scale of the experiment that is governed by the sweep rate: the higher the sweep rate, the smaller the kinetic contribution to the current (Figure 1b). Reaction 2 must thus be replaced by the scheme shown in reaction 2'.

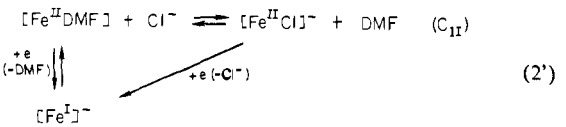

(2')

When passing to aPF (Figure 9), it is noteworthy that the anodic wave of the first wave system is now reversible even without adding chloride ions to the solution. Correlatively, the second wave system exhibits when the sweep rate is raised two cathodic waves instead of one also without purposely added Cl^-. The second cathodic wave increases at the expense of the first upon addition of Cl^- and/or increases in the sweep rate in accordance with the above reaction scheme. These two observations point to the conclusion that the substitution of DMF by Cl^- in the ferrous complex is quite significantly increased when passing from TPP to aPF.

The cyclic voltammetry of the three amide-linked basket-handle porphyrins exhibits the same trends as aPF when compared to TPP. The $[Fe^{I}]^-/[Fe^{I}\cdot]^{2-}$ is more easily reversible than with TPP, and its standard potential is shifted positively. The values of the latter quantity are listed in Table IV. The changes of both the first and second wave systems reveal a larger affinity of Fe^{II} for Cl^- in reaction C_{II} than with TPP.

Association of Cl^- to Fe^{II} is now actually so large that the anodic waves of the first wave system are no longer an appropriate source of data for investigating quantitatively the thermodynamics and kinetics of reaction C_{II} unlike what was done in the case of ether-linked basket-handle compounds. It is now preferable to have recourse to the cathodic waves of the second wave system (Fe^{II}/Fe^{I}) for determining the rate constants of reaction C_{II}, taking advantage of the occurrence of a CE mechanism at the Fe^{II}/Fe^{I} level as pictured above. This is again opposite to what was ob-

Table IV. Electrochemical Characteristics of the Reduction to $Fe^{III}Cl$ Amide-Linked Basket-Handle and Picket-Fence Porphyrins As Compared to 5,10,15,20-Tetraphenylporphyrin in DMF

	reaction 1				reaction 2		reaction 3	
	$E^\circ_{[Fe^{III}Cl]/[Fe^{II}Cl]^-}$[a]	K_A^{II}[b]	k_a^{II}[c]	k_d^{II}[d]	$E^\circ_{[Fe^{II}DMF]/[Fe^{I}]^-}$[a]	$\Delta E^\circ_{[Fe^{II}DMF]/[Fe^{I}]^-}$[e]	$E^\circ_{[Fe^{I}]^-/[Fe^{I}]^{2-}}$[a]	$\Delta E^\circ_{[Fe^{I}]^-/[Fe^{I}]^{2-}}$[e]
TPP	−0.191	56	1.0×10^5	2.0×10^3	−0.984		−1.680	
a(C12)$_2$-CT	−0.138 (53)	1200	2.1×10^5	1.9×10^2	−0.887 (97)	164	−1.530 (150)	330
a(C12)$_2$-AT	−0.074 (117)	3000	1.2×10^7	3.9×10^3	−0.874 (110)	145	−1.505 (175)	270
a(C12)$_2$-AC	−0.118 (73)	1800	1.8×10^6	1.0×10^3	−0.873 (111)	151	−1.455 (225)	300
aPF	−0.103 (88)	3600	1.2×10^5	3.3×10^1	−0.837 (147)		−1.440 (240)	

[a] Standard potential in V vs. NaCl SCE; the distance in mV from the E° corresponding to TPP is given in parentheses. [b] Association equilibrium constant of Fe^{II} with Cl^- in M^{-1}. [c] Association rate constant of Fe^{II} with Cl^- in $M^{-1}\ s^{-1}$. [d] Dissociation rate constant in s^{-1}. [e] $(E^\circ_{aC12} - E^\circ_{TPP}) + (E^\circ_{TAP} - E^\circ_{eC12})$.

Table V. Spectral Characteristics of the DMF and Ferrous Chloro Complexes of TPP and Amide-Linked Basket-Handle and Picket-Fence Porphyrins

	Soret region λ_{max}, nm $\epsilon \times 10^{-4}$, $M^{-1}\ cm^{-1}$		visible region λ_{max}, nm[a]	
	$[Fe^{II}DMF]$	$[Fe^{II}Cl]^-$	$[Fe^{II}DMF]$	$[Fe^{II}Cl]^-$
TPP	430 (16.2)	441 (18.0)	532, 562, 604	530, 570, 610
a(C12)$_2$-CT	438 (15.0)	446 (21.8)	534, 565, 610	529, 572, 612
a(C12)$_2$-AT	436 (19.2)	446 (23.6)	534, 566, 608	528, 570, 611
a(C12)$_2$-AC	435 (27.2)	444 (26.0)	530, 565, 604	520, 569, 608
aPF	434 (19.6)	445 (22.8)	532, 566, 608	528, 569, 609

[a] The ϵ in the visible range could not be determined accurately in this work.

served with the ether-linked basket-handle compounds where the coordination of Fe^{II} by Cl^- was too weak for such a procedure to be conveniently followed.

We thus used the variations of the ratio between the peak height of the first cathodic wave of the second wave system (reduction of $[Fe^{II}DMF]$ and the peak height corresponding to a one-electron diffusion-controlled process with the chloride ion concentration and the sweep rate for determining the rate constants of reaction C_{II}. The procedures we employed are described in detail elsewhere.[14b,20a] They require that the equilibrium constant for the association of Cl^-, K_A^{II}, be known independently. We used, as previously,[14b] thin-layer spectroelectrochemistry for this purpose.

Figure 10 shows a typical spectroelectrochemical experiment. Solutions of the a(C12)$_2$-AT iron(III) chloro complex containing increasing amounts of LiCl were electrolyzed at −0.7 V vs. NaCl SCE, and the spectra were recorded (parts a and b of Figure 10). The plot of $1/(D - D_0)$ vs. $1/[Cl^-]$ (Figure 10c) obeys eq 4, where

$$\frac{1}{D - D_0} = \frac{1}{K_A^{II}} \frac{1}{D_\infty - D_0} \frac{1}{[Cl^-]} + \frac{1}{D_\infty - D_0} \qquad (4)$$

D is the observed absorbance and D_0 and D_∞ are the absorbances corresponding to $[Fe^{II}DMF]$ and $[Fe^{II}Cl]^-$, respectively. An expression including $1/(D - D_0)$ was chosen rather than $1/(D - D_\infty)$ because at strong concentrations of Cl^-, it seems that a second Cl^- is added to the complex and D_∞ is thus inaccurate. $D_\infty - D_0$ is obtained from the intercept and K_A^{II} from the slope of the resulting straight line. All the other porphyrins show the same behavior. Their spectral characteristics are given in Table V and the values of K_A^{II} thus measured in Table IV.

Once K_A^{II} is known, the above described cyclic voltammetric data can be treated[14b,20a] to obtain the association and dissociation rate constants of reaction C_{II}. The results are given in Table IV.

Two other standard potentials of interest can be derived by using the spectrometricaly measured values of K_A^{II}. At sufficiently large concentrations of Cl^-, the first wave system involves a single reversible wave, corresponding to rapid equilibration of reaction C_{II} within the time scale of the experiments. The resulting apparent standard potential $E^\circ_{III/II}{}^{ap}$ is then related to the standard potential of the $[Fe^{III}Cl]/[Fe^{II}Cl]^-$ couple through[20a]

$$E^\circ_{III/II}{}^{ap} = E^\circ_{|Fe^{III}Cl|/|Fe^{II}Cl|^-} - (RT/F) \ln \{K_A^{II}[Cl^-]/(1 + K_A^{II}[Cl^-])\}$$

It is thus possible to derive, knowing K_A^{II}, $E^\circ_{|Fe^{III}Cl|/|Fe^{II}Cl|^-}$ (Table IV) from the measured values of the apparent standard potential.

On the other hand, at low sweep rates and Cl^- concentrations, the second wave system exhibits a single reversible wave corresponding to rapid equilibration of reaction C_{II} toward the reduction of $[Fe^{II}DMF]$ within the time scale of the experiment. The corresponding apparent standard potential $E^\circ_{II/I}{}^{ap}$ is then given in eq 5 from which the values of the standard potential $E^\circ_{|Fe^{II}DMF|/|Fe^{I}|^-}$ were derived (Table IV) knowing K_A^{II}.[26]

$$E^\circ_{II/I}{}^{ap} = E^\circ_{|Fe^{II}DMF|/|Fe^{I}|^-} - (RT/F) \ln \{1 + K_A^{II}[Cl^-]\} \qquad (5)$$

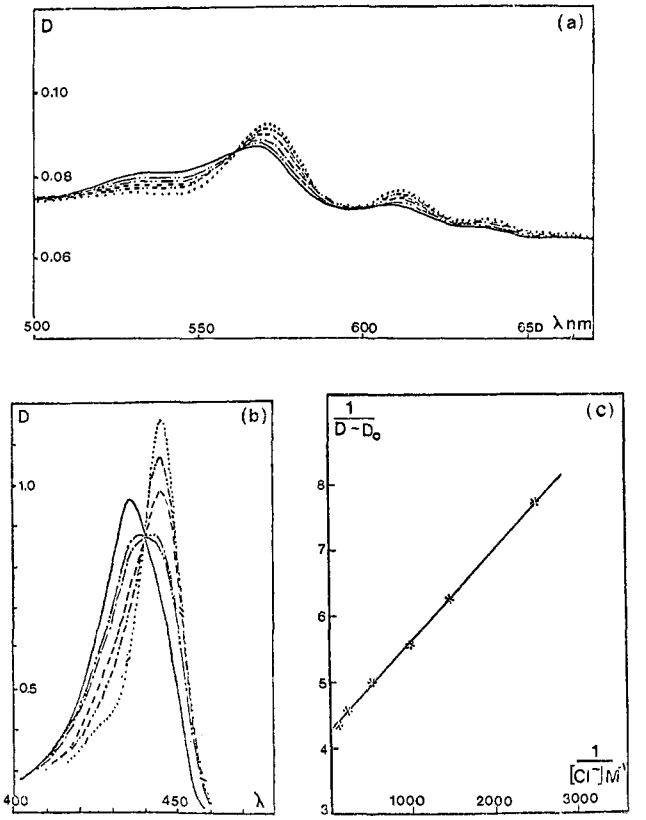

Figure 10. Thin-layer spectroelectrochemistry of $ClFe^{III}a(C12)_2$-AT (0.05 mM) in DMF + 0.1 M $LiClO_4$ [LiCl concentration, 0 (—), 1 mM (-·-·-), 2.4 mM (-·-), 4.0 mM (---), 10 mM (-·····), 100 mM (···); electrolysis potential: −0.7 V vs. NaCl SCE]: (a) visible region, (b) Soret region, (c) determination of K_A^{II}, D = Cl^--dependent absorbance; D_0 = absorbance corresponding to Fe^{II} DMF.

Table VI. Standard Potentials of the $[Fe^{I}]^{-}/[Fe^{I}\cdot]^{2-}$ Redox Couples as a Function of the Solvent[a]

	solvent		
	DMF	DMA	PhCN
TPP	−1.680	−1.620	−1.690
$a(C12)_2$-CT	−1.530 (150)	−1.460 (160)	−1.660 (30)
aPF	−1.440 (240)	−1.410 (210)	−1.600 (90)

[a] The distance in mV from the $E°$ corresponding to TPP is given in parenthesis.

The kinetics of the reduction of $[Fe^{II}Cl]^{-}$ into $[Fe^{I}]^{-}$ show remarkable variations among the five porphyrins. The $a(C12)_2$-AT and $a(C12)_2$-AC complexes give rise to two cathodic peaks of the second wave system that are much closer at a given sweep rate than in the case of TPP and aPF. The $a(C12)_2$-CT isomer exhibits a behavior very similar to that of TPP and aPF. The differences of K_A^{II} between the various protected porphyrins are not such to explain this phenomenom which therefore reflects variations in the kinetics of the reduction of the $[Fe^{II}Cl]^{-}$ complex. This is significantly faster with $a(C12)_2$-AT and $a(C12)_2$-AC than with TPP, $a(C12)_2$-CT, and aPF.

Additional Experiments. Variations with the Solvent. In order to gain further insight into the role of the solvent in the observed effects of the protecting chains, we carried out a few additional experiments in benzonitrile (PhCN) and dimethylacetamide (DMA). The general electrochemical behavior was the same as in DMF. Chloride ion association appears qualitatively significantly larger in PhCN and about the same in DMA as expected from the ligation properties of these molecules as compared to DMF. The quantitative observations were limited to the standard potentials of the $[Fe^{I}]^{-}/[Fe^{I}\cdot]^{2-}$ derived from the location of the reversible "ring wave" (Table VI). The experiments were carried out with 0.1 M NEt_4ClO_4 as the supporting electrolyte in PhCN and 0.1 M NBu_4BF_4 in DMA. It was checked on several examples in DMF that the location of the reversible ring wave is practically independent of the nature of the cation of the supporting electrolyte (Li^+, NEt_4^+, NBu_4^+).

Discussion. The most striking feature of the results described above is the parallelism between the effects of the chains on the thermodynamics of reactions C_{II}, 2, and 3: when passing from TPP to the basket-handle and picket-fence porphyrins, chloride association to Fe^{II} increases and reductions of $[Fe^{II}DMF]$ into $[Fe^{I}]^{-}$ and of $[Fe^{I}]^{-}$ into $[Fe^{I}\cdot]^{2-}$ become easier. A common characteristic of these three reactions is that the negative charge of the reactants increases by one unit from the left-hand to the right-hand side. The presence of the amide-linked chains thus stabilizes the negatively charged species: $[Fe^{II}Cl]^{-}$ is stabilized toward $[Fe^{I}DMF]$, $[Fe^{I}]^{-}$ toward $[Fe^{II}DMF]$, and $[Fe^{I}\cdot]^{2-}$ toward $[Fe^{I}\cdot]^{-}$. It is noteworthy that the influence of ether-linked basket-handle chains of the identical structure is exactly the opposite: as compared to the unprotected complex the thermodynamics of the same three reactions vary in the converse direction. Comparing the figures given in Table IV to those of Table I, it is seen that passing from an amide-linked to an ether-linked basket-handle compound results in variations that can be as large as 5 orders of magnitude in terms of equilibrium constant, i.e., 0.3 eV in terms of free energy. It was shown that the effects of the ether-linked basket handles are essentially due to steric hindrance to solvation of the negatively charged species by the chains. In the case of amide-linked chains we are thus led to relate the observed effects to a specific influence of the NHCO groups stabilizing the negatively charged species. Hydrogen bonding by the amide hydrogen, as in the case of iron(II) dioxygen adducts,[8c,10] and/or dipole–charge interactions appear as likely causes of the stabilizing effect.

Reaction 3 is expected to give rise to the largest effects since it involves the formation of a doubly charged species from a singly charged species. This is indeed the case in DMF as can be seen in Table IV. When attempting to estimate the stabilizing role of the NHCO groups, we have to take into account that stabilization of the negatively charged species by the solvent is much larger in TPP than in the protected porphyrins due to steric hindrance to solvation by the chains as demonstrated in the case of ether-linked basket-handle compounds. This clearly appears in the present case through the comparison between the porphyrins that are protected on only one face ($a(C12)_2$-AC, aPF) with those that are protected on both faces ($a(C12)_2$-CT, $a(C12)_2$-AT). The shift of the standard potential with reference to TPP is significantly larger with the former than with the latter compounds. Solvation of the negatively charged species by the solvent being less hindered helps stabilization more in the first case than in the second. In this context, an estimate of the specific stabilizing effect of the NHCO groups is obtained by adding the $E°$ shifts observed between the amide-linked basket-handle porphyrins and TPP to the $E°$ shifts observed between TAP and the ether-linked basket-handle porphyrins, the latter term being an approximate measure of steric hindrance to solvation. The sum thus obtained is approximately constant in the series, being on the order of 300 mV. This is actually a minimal estimation of the stabilizing effect of the NHCO groups in reaction 3 for two reasons. First, as discussed before, the choice of TAP as reference compound for the ether-linked series may lead to an overestimation of the electronic effect of the ether groups that would result in a slight underestimation of the term $E°_{TAP} - E°_{eC12}$. On the other hand, the choice of TPP as reference compound for the amide-linked series may lead to a slight underestimation of the NHCO groups: the restricted rotation around the porphyrin ring–phenyl bond in the case of the superstructured porphyrins may forbid any conjugation between the phenyl groups and the porphyrins contributing to a negative shift of the $E°$'s as compared to TPP. The NHCO stabilizing effect in reaction 3 may thus be slightly larger, but not smaller, than 300 mV, i.e., 5 orders of magnitude in terms of equilibrium constants or 7 kcal/mol for the four amide groups, i.e., approximately 2 kcal/mol/amide group.

As regards to reaction 2 the same procedure leads to a specific effect of the amide groups of about 150 mV (Table IV). In the case the addition of the $E°_{TAP} - E°_{eC12}$ terms takes care both for steric hindrance of solvation by the chains and steric destabilization of the DMF ligand. If, in their stabilizing action, the amide groups were regarded as fixed dipoles, the $\Delta E°$ should be same for reactions 2 and 3. If the amide dipoles were randomly distributed, $\Delta E°$ for reaction 3 should be three times $\Delta E°$ for reaction 2 owing to polarization by the negative charges. We find an intermediate ratio (ca. 2) indicating partial polarization of the amide dipoles that undergo a restricted spatial orientation under the influence of the negative charges. Variations of the dipole moments from inducement by the negative charges may also play a role in the stabilization mechanism.

Another interesting observation results from the comparison of the $E°$ shifts in DMF, DMA, and benzonitrile (Table VI). It is seen that the shifts are about the same in DMF and DMA and are smaller in PhCN, the order $a(C12)_2$-CT < aPF being conserved. This points to the concept that a solvent molecule may be present inside the cage formed by the chains serving as a relay for the stabilization of the negative charge delocalized over the iron atom and the porphyrins ring by the H atom of the amide group. DMF and DMA would be more efficient in this respect than PhCN, giving rise to stronger H bonding with NHCO through their oxygen atom. Steric interactions with the chains would result in lesser efficiency of DMA as compared to DMF that could, however, be compensated by the electron-donating effect of the methyl group, leading to stronger H bonding of the oxygen atom in DMA than in DMF. A more systematic investigation of the series of amide-linked superstructured porphyrins as a function of the nature of the solvent should, however, be undertaken in order to confirm or dismiss this point as opposed to an interpretation that would regard dipole–charge interactions as the major cause of the stabilizing effect.

Large positive shifts of the $E°$ of reaction 2 are also observed when passing from TPP to the amide-linked basket-handle and

(26) In the case where it is necessary to use the data from experiments with no added Cl^- for this purpose (this is in fact true for all the protected porphyrins) $K_A^{II}[Cl^-]$ is replaced by the ratio of the chloro and DMF complex concentrations calculated from the dissociation coefficient.

picket-fence porphyrins in DMF (Table IV). The magnitude of the shift varies only a little from one protected porphyrin to the other. This suggests that the amide groups are responsible for most of the stabilization of the singly charged $[Fe^{I}]^-$ complexes with little participation of solvation from the surrounding solvent in the protected porphyrins.

$[Fe^{II}Cl]^-$ is significantly stabilized toward $[Fe^{II}DMF]$ by the presence of the amide-linked chains. Here again K_A^{II} does not vary significantly among the various protected compounds, suggesting that stabilization of the negative charge in $[Fe^{II}Cl]^-$—which is presumably more concentrated than in $[Fe^{I}]^-$ and $[Fe^{I}\cdot]^{2-}$—is mostly caused by the amide groups without major involvement of the surrounding solvent in the protected complexes. The exact nature of the stabilization of the chloro complex by the NHCO groups is not known.

The standard potentials of the reduction of $[Fe^{III}Cl]$ to $[Fe^{II}Cl]^-$ also show substantial positive shifts when passing from TPP to the protected porphyrins. They approximately parallel the variations of K_A^{II}, suggesting that the predominant effect of the amide-linked chains is, here too, the stabilization of the negatively charged $[Fe^{II}Cl]^-$ complex by the NHCO groups.

From a kinetic point of view the main differences are not between TPP, on one hand, and the group of protected porphyrins, on the other. Rather the $a(C12)_2$-AT and $a(C12)_2$-AC complexes appear to behave differently from the three other porphyrins. When passing from TPP to $a(C12)_2$-CT or aPF, the rate constant for the association of Cl^- to Fe^{II} remains about the same while the dissociation rate constant decreases. With the AT and AC isomers both association and dissociation are much faster, by 1 or 2 orders of magnitude, than those with the CT isomer and the picket-fence porphyrins. The very same trends were observed with the ether-linked basket-handle porphyrins of similar structure. In both cases the AT and AC isomers appear as "more rapid", suggesting that the flexibility of the chains in these compounds induces a more facile replacement of one ligand by the other by sterically promoting four-coordinate intermediates or transition states. This also falls in line with the observation that the electron transfer to $[Fe^{II}Cl]^-$ was observed to be significantly faster with the AT and AC isomers than with the other three porphyrins.

Concluding Remarks

Several important conclusions emerge from the preceding discussion of the influence of basket-handle and picket-fence structures on the redox and coordination chemistry of iron porphyrins.

The predominant effect of the ether-linked basket-handle chains is to sterically hinder solvation by polar solvents of the negatively charged complexes. This renders the three successive reduction processes $[Fe^{III}Cl]$ to $[Fe^{II}Cl]^-$, $[Fe^{II}DMF]$ to $[Fe^{I}]^-$, and $[Fe^{I}]^-$ to $[Fe^{I}\cdot]^{2-}$ more difficult to an extent which is an increasing function of the effective solvation radius offered by the conformational arrangement of the chains. It also decreases the substitution of a DMF molecule by a chloride ion in the Fe^{II} complexes.

In addition, steric interactions between the chains and the axial ligands manifest themselves in the thermodynamics of the reduction of $[Fe^{II}DMF]$ to $[Fe^{I}]^-$ as well as of the Cl^-/DMF substitution reaction in the ferrous complexes.

While the presence of ether-linked chains destabilizes the negatively charged species by steric hindrance to solvation by polar solvents, the amide-linked chains conversely induce a quite significant stabilization of the same negatively charged complexes. In the latter case, this is revealed by the fact that the three successive reduction processes $[Fe^{III}Cl] \rightarrow [Fe^{II}Cl]^-$, $[Fe^{II}DMF] \rightarrow [Fe^{I}]^-$, and $[Fe^{I}]^- \rightarrow [Fe^{I}\cdot]^{2-}$ are facilitated and so is chloride ion association to Fe^{II}, while the ether-linked chains produce strictly opposite effects. Specific stabilization by the NHCO groups is estimated as being of the order of 0.3 eV, i.e., 5 orders of magnitude in terms of the equilibrium constant, for reaction 3 and 0.15 eV for reaction 2.

Hydrogen bonding involving the hydrogen atom of the NHCO groups and/or dipole–charge interactions appear responsible for these microenvironment effects. Amide-linked superstructured porphyrins thus behave like "snail" or "turtle" molecules carrying their own solvent on their back.

Steric interactions play an important role in the kinetics of ligand exchange at Fe^{II}. The protected complexes involving the most flexible chains, able to be compressed toward the porphyrin ring, give rise to the fastest exchange reactions as already observed with similar ether-linked structures. The same steric effects also interfere in the rate of electron transfer to the $[Fe^{II}Cl]^-$ complexes.

It is tempting to speculate that polar interactions similar to those observed in the amide-linked series may take place in metalloenzymes where the prosthetic group may come close to a number of NHCO groups belonging to the surrounding protein chains.[29] Such interactions might then contribute to the tuning of the redox and coordination properties of the metal center. Conversely, they might affect the conformation of the protein chains thus participating to cooperativity and allosteric effects.

Experimental Section

Chemicals. The basket-handle, picket-fence, and TAP iron(III) chloride complexes were synthesized and characterized according to already described procedures.[2a,8,27,28] $Fe^{III}TPPCl$ was from commercial origin and was used as received.

Reagent grade DMF from Merck and Carlo Erba was used. In the first case, it was distilled before use and stored on 4-Å molecular sieves. The Carlo Erba DMF contained less than 0.05% water and was used in the experiments designed to accurately measure the standard potential of the "ring wave". Benzonitrile was a reagent grade Merck product. It was distilled and passed over neutral alumina before use.

$LiClO_4$ and LiCl were reagent grade products (Fluka). They were dried before use. NBu_4BF_4 (Fluka, puriss) was used as received.

Cyclic Voltammetry. A three-electrode configuration contained in a conical inactinic glass cell equipped with a water jacket was used with a volume of solution of 5 cm^3. The temperature of all experiments was 20 ± 1 °C. The solutions were purged with argon, and an argon atmosphere was maintained during the experiments. The counterelectrode was a platinum wire. The reference electrode was an NaCl-saturated calomel electrode. All potentials are referred to this electrode throughout the paper. NaCl was used instead of KCl to prevent the precipitation of ClO_4K (when having a perchlorate as supporting electrolyte in the solution) in the pores of the glass frit separating the reference electrode compartment from the bridge containing the same solvent and supporting electrolyte as the solution under investigation. The potential of the NaCl SCE is 5.5 mV negative to that of the KCl SCE.[24a] The working electrode was a glassy carbon disk electrode obtained by sealing in a glass holder a 3-mm diameter rod. The carbon disk was frequently polished by using diamond pastes of decreasing sizes (7, 3, 1 μm) followed by ultrasonic washing with ethanol and drying.

The instrumentation was composed of a home-built potentiostat equipped with a positive feedback IR compensation,[24b] a PAR Model 175 function generator, an IFFELEC IF 2502 XY pen recorder, and a SCHLUMBERGER A 220 digital voltmeter. The peak potentials were measured with an accuracy of about ±3 mV.

The determination of the rates constants of reaction C_{II} was carried out from the height of the $[Fe^{II}Cl^-]$ anodic wave normalized to the height corresponding to a one-electron diffusion-controlled wave. The latter was obtained when a great excess of chloride anions was present that lead to a $[Fe^{II}Cl]^-$ wave the height of which is proportional to the square root of the sweep rate within the investigated range. The value of the $[Fe^{II}Cl]^-/[\text{total } Fe^{II}]$ ratio is obtained for each $[Cl^-]$ concentration from the value of K_A^{II} determined spectrochemically (vide infra). Working curves relating the above peak/current ratio to the kinetic parameter $\lambda = (k_a[Cl^-] + k_d)(RT/Fv)$ (v is the sweep rate) were generated for each value of the Fe^{II} concentration ratio on a Mini 6 CII computer using already described theory and computation procedures.[20a]

Spectroelectrochemistry. The three-electrode thin-layer cell was of the same type as previously described.[24c] The height of the thin-layer part was 2 cm and its internal width 0.05 cm. The working electrode was a platinum grid. The reference electrode was the same as that in cyclic voltammetry. The cell was thermostated at a temperature of 20 ± 1 °C. The working electrode potential was set by a ±10-V, 18-mA potentiostat similar to that used in cyclic voltammetry. The determination of K_A^{II}

(27) Collman, J. P.; Gagne, R. R.; Halbert, T. R.; Marchon, J. C.; Reed, C. A. *J. Am. Chem. Soc.* **1973**, *95*, 7860.
(28) Momenteau, M.; Loock, B.; Mispelter, J., submitted for publication.
(29) (a) Such effects have indeed been observed in iron–sulfur proteins.[29b,c] (b) Sweeny, W. V.; Rabinowitz, J. C.; *Ann. Rev. Biochem.* **1980**, *49*, 139. (c) Carter, C. W.; *J. Biol. Chem.* **1977**, *252*, 7802.

was carried out according to standard procedures[24d] using as a reference spectrum that of the [Fe^{II}DMF] complex. The spectral characteristics of the [Fe^{II}DMF] and [$Fe^{II}Cl]^-$ complexes in the Soret region are given in Table II. The molecular extinction coefficients of the two complexes at their respective maximum of absorption exhibit usual values ((2–4) $\times 10^5$ M^{-1} cm^{-1}).

Acknowledgment. This work was supported in part by the CNRS (Equipe de Recherche Associée 309 "Electrochimie Moléculaire").

Registry No. DMF, 68-12-2; Fe^{III}(TAP)Cl, 90837-94-8; Fe^{III}(e-$(C12)_2$-AC)Cl, 90837-95-9; Fe^{III}(e$(C12)_2$-AT)Cl, 90898-37-6; Fe^{III}(e-$(C12)_2$-CT)Cl, 79198-03-1; Fe^{III}(e[di(C4)Ph]$_2$-CT)Cl, 83460-51-9; $[Fe^{III}(TAP)Cl]^-$, 90837-96-0; $[Fe^{II}(e(C12)_2\text{-}AC)Cl]^-$, 90837-97-1; $[Fe^{II}(e(C12)_2\text{-}AT)Cl]^-$, 90898-38-7; $[Fe^{II}(e(C12)_2\text{-}CT)Cl]^-$, 90837-98-2; $[Fe^{II}(e[di(C4)Ph]_2\text{-}CT)Cl]^-$, 90837-99-3; $[Fe^{I}(TAP)]^-$, 90838-00-9; $[Fe^{I}(e(C12)_2\text{-}AC)]^-$, 90838-01-0; $[Fe^{I}(e(C12)_2\text{-}AT)]^-$, 90838-02-1; $[Fe^{I}(e(C12)_2\text{-}CT)]^-$, 79209-91-9; $[Fe^{I}(e[di(C4)Ph]_2\text{-}CT)]^-$, 90838-03-2; $[Fe^{I}\cdot(TAP)]^{2-}$, 90838-04-3; $[Fe^{I}\cdot(e(C12)_2\text{-}AC)]^{2-}$, 90838-05-4; $[Fe^{I}\cdot(e(C12)_2\text{-}AT)]^{2-}$, 90898-39-8; $[Fe^{I}\cdot(e(C12)_2\text{-}CT)]^{2-}$, 90838-06-5; $[Fe^{I}\cdot(e[di(C4)Ph]_2\text{-}CT)]^{2-}$, 90838-07-6; Fe^{II}(DMF)(TAP), 90838-08-7; Fe^{II}(DMF)(e$(C12)_2$-AC), 90838-09-8; Fe^{II}(DMF)(e$(C12)_2$-AT), 90898-40-1; Fe^{II}(DMF)(e$(C12)_2$-CT), 90838-10-1; Fe^{II}(DMF)(e[di(C4)-Ph]$_2$-CT), 90838-11-2; Fe^{III}(TPP)Cl, 16456-81-8; Fe^{III}(a$(C12)_2$-CT)Cl, 90838-12-3; Fe^{III}(a$(C12)_2$-AT)Cl, 90838-13-4; Fe^{III}(a$(C12)_2$-AC)Cl, 90898-41-2; Fe^{III}(aPF)Cl, 86107-94-0; $[Fe^{II}(TPP)Cl]^-$, 84537-58-6; $[Fe^{II}(a(C12)_2\text{-}CT)Cl]^-$, 90838-14-5; $[Fe^{II}(a(C12)_2\text{-}AT)Cl]^-$, 90838-15-6; $[Fe^{II}(a(C12)_2\text{-}AC)Cl]^-$, 90898-42-3; $[Fe^{II}(aPF)Cl]^-$, 86124-06-3; Fe^{II}-(DMF)(TPP), 90838-16-7; Fe^{II}(DMF)(a$(C12)_2$-CT), 90838-17-8; Fe^{II}(DMF)(a$(C12)_2$-AT), 90838-18-9; Fe^{II}(DMF)(a$(C12)_2$-AC), 90898-43-4; Fe^{II}(DMF)(aPF), 90838-19-0; $[Fe^{I}(TPP)]^-$, 54547-68-1; $[Fe^{I}(a(C12)_2\text{-}CT)]^-$, 90838-20-3; $[Fe^{I}(a(C12)_2\text{-}AT)]^-$, 90838-21-4; $[Fe^{I}(a(C12)_2\text{-}AC)]^-$, 90898-44-5; $[Fe^{I}(aPF)]^-$, 90857-60-6; $[Fe^{I}\cdot(TPP)]^{2-}$, 90838-22-5; $[Fe^{I}\cdot(a(C12)_2\text{-}CT)]^{2-}$, 90838-23-6; $[Fe^{I}\cdot(a(C12)_2\text{-}AT)]^{2-}$, 90838-24-7; $[Fe^{I}\cdot(a(C12)_2\text{-}AC)]^{2-}$, 90898-45-6; $[Fe^{I}\cdot(aPF)]^{2-}$, 90838-25-8; $LiClO_4$, 7791-03-9; NBu_4BF_4, 429-42-5; chlorine, 7782-50-5.

Hemocyanin Models: Synthesis, Structure, and Magnetic Properties of a Binucleating Copper(II) System

Vickie McKee, Maruta Zvagulis, Jeffrey V. Dagdigian, Marianne G. Patch, and Christopher A. Reed*

Contribution from the Department of Chemistry, University of Southern California, Los Angeles, California 90089. *Received December 29, 1983*

Abstract: A model compound approach to oxidized hemocyanin is described. The essential structural features of diamagnetism, 3.6-Å copper–copper separation, approximate tetragonal stereochemistry, imidazole ligation, and bridging groups are reproduced in the azide complex $[Cu_2(L\text{-}Et)(N_3)][BF_4]_2$. HL-Et is the septadentate binucleating ligand *N,N,N′,N′*-tetrakis(2-(1-ethylbenzimidazolyl))-2-hydroxy-1,3-diaminopropane prepared in good yield via condensation of 1,2-diaminobenzene with 2-hydroxy-1,3-diaminopropanetetraacetic acid. Related complexes $[Cu_2(L\text{-}Et)X]^{2+}$ where X^- = OAc^-, $HCOO^-$, NO_2^-, and pyrazolate have quite different magnetic properties. The acetate is ferromagnetic ($J \simeq +12$ cm^{-1}) while the nitrite is antiferromagnetic ($J = -139$ cm^{-1}). Crystal structures of the weakly coupled acetate complex $[Cu_2(L\text{-}Et)(OAc)][ClO_4]_2$ (monoclinic, $P2_1/n$, $a = 14.190$ (3) Å, $b = 22.707$ (4) Å, $c = 15.883$ (4) Å, $\beta = 97.20$ (2)°, $Z = 4$) and the diamagnetic azide complex $[Cu_2(L\text{-}Et)(N_3)][BF_4]_2$ (monoclinic, $C2/m$, $a = 19.082$ (3) Å, $b = 23.896$ (3) Å, $c = 13.230$ (2) Å, $\beta = 116.21$ (1)°, $Z = 4$) suggest that these differences have their origin in the orientation of the σ magnetic orbitals with respect to the bridging ligands. The particular mode of 1,3-bridging azide in $[Cu_2(L\text{-}Et)(N_3)]^{2+}$, where it is supported by an alkoxide bridge from L-Et, has not been previously observed. It allows close approach of the copper(II) atoms (3.615 (3) Å) and thus becomes a viable stereochemistry for metazidohemocyanin. The present studies support the idea that tetragonality of the copper(II) stereochemistry is important for attaining diamagnetism in oxy- and methemocyanins and that alkoxide from serine or threonine would be well suited to the role of a bridging endogenous ligand.

A long-standing problem in bioinorganic chemistry is understanding how hemocyanin[1] functions as an oxygen carrier. The operative states of this dinuclear copper protein are the colorless Cu(I) deoxy form, Hc, and the blue Cu(II) oxy form, HcO_2. Their structures are modestly well-defined by a recent accumulation of chemical and spectroscopic data such that Scheme I, with some caveats, can be adopted as a working model.

For the deoxy state, the essential spectroscopic invisibility of Cu(I) leaves mainly EXAFS studies[2,3] and its reactivity with carbon monoxide[4] as a guide to structure. While the precise coordination number and stereochemistry are unknown, it is known that there are at least two histidines per copper and some form

Scheme I. Possible Structures for Various States of Hemocyanin[a]

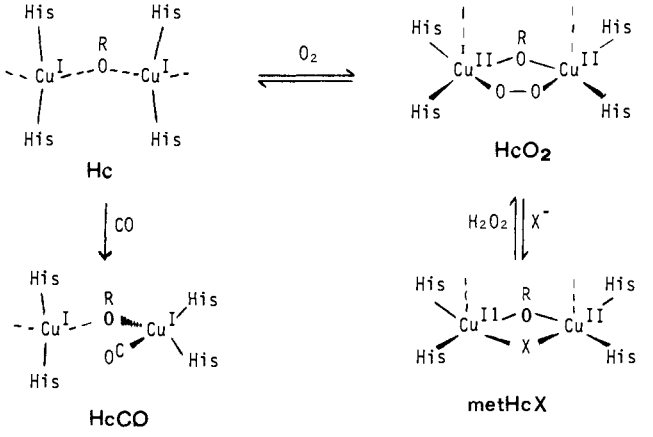

[a] Dashed lines are used to indicate uncertainty in coordination number.

(1) For reviews on hemocyanin see: (a) van Holde, K. E.; Miller, K. I. *Q. Rev. Biophys.* **1982**, *15*, 1–129. (b) Lontie, R.; Witters, In "Inorganic Biochemistry"; Eichhorn, G. L., Ed.; Elsevier: New York, 1973; Vol. 1, Chapter 12; (c) Lontie, R.; Vanquickenborne, L. In "Metal Ions in Biological Systems" Siegel, H., Ed.; Marcel Dekker: New York, 1974; Vol. 3, pp 183–200. (d) Senozan, N. M. *J. Chem. Educ.* **1976**, *53*, 684–688. (e) Solomon, E. I. In "Metal Ions in Biology"; Spiro, T. G., Ed.; Wiley-Interscience: New York, 1981; Vol. 3, pp 41–108. (f) Bonaventura, J.; Bonaventura, C. *Am. Zool.* **1980**, *20*, 7–17. (g) Owen, C. A. "Biochemical Aspects of Copper"; Noyes: New Jersey, 1982; pp 41–48.

(2) (a) Brown, J. M.; Powers, L.; Kincaid, B.; Larrabee, J. A.; Spiro, T. G. *J. Am. Chem. Soc.* **1980**, *102*, 4210–4216. (b) Woolery, G. L.; Powers, L.; Winkler, M.; Solomon, E. I.; Spiro, T. G. *Ibid.* **1984**, *106*, 86–92.

(3) Co, M. S.; Scott, R. A.; Hodgson, K. O. *J. Am. Chem. Soc.* **1981**, *103*, 986–988.

0002-7863/84/1506-4765$01.50/0